

Proceedings of the CTD/WIT 2019
 PROC-2019-XXX
 December 26, 2022

GPGPU Tracking in the COMET Phase-I Cylindrical Drift Chamber

BEOMKI YEO

*Department of Physics,
 Korea Advanced Institute of Science and Technology, Republic of Korea*

MYEONG JAE LEE, YANNIS K. SEMERTZIDIS

*Center for Axion and Precision Physics Research,
 Institute for Basic Science (IBS), Daejeon 34051, Republic of Korea*

YOSHITAKA KUNO

*Department of Physics, Graduate School of Science,
 Osaka University, Toyonaka, Osaka 560-0043, Japan*

ABSTRACT

The track finding with GPGPU-implemented fourth order Runge-Kutta (RK) method is investigated to track electrons from muon decay in the COMET Phase-I cylindrical drift chamber. The COMET Phase-I experiment is aiming for discovering the neutrinoless, coherent transition of a muon to an electron in the field of an aluminium nucleus, $\mu^- + N \rightarrow e^- + N$, with a single event sensitivity of 3.1×10^{-15} . In the COMET cylindrical drift chamber, about 30% of signal events are composed of multiple turns where the correct hit assignments to each turn partition are significant in the track finding. Scanning all possible track seeds can resolve the hit-to-track assignment problem with a high robustness against the noise hits, but requires a huge computational cost; initial track seeds $(\theta, z, p_x, p_y, p_z)$ have broad uncertainties, so many initial seeds should be tried and compared. In this presentation, this problem of massive computations are mitigated with 1) the parallel computing of RK track propagation, which assigns each track to each GPU block unit, 2) a better initial guess on the track seeds using the Hough transform and the geometrical property of the cylindrical drift chamber. The computation speed enhancement compared to CPU-only calculation is also presented.

PRESENTED AT

Connecting the Dots and Workshop on Intelligent Trackers (CTD/WIT 2019)
 Instituto de Física Corpuscular (IFIC), Valencia, Spain
 April 2-5, 2019

1 Introduction

1.1 COMET experiment

The COMET experiment [4], located at J-PARC in Japan, will investigate the neutrinoless muon to electron conversion ($\mu^- + N \rightarrow e^- + N$) in a muonic atom. Its single event sensitivities in Phase-I and Phase-II are 3.1×10^{-15} and 2.6×10^{-17} , respectively, which are about 100 and 10000 times enhancement compared to the latest experimental upper limit of 7×10^{-13} [1]. In the Phase-I experiment, the proton beam from J-PARC accelerator hits the production target to generate the pions which decay into muons subsequently (see Fig. 1). Those muons are transported along the solenoid. Afterwards, they enter the detector region called CyDet and are stopped by the aluminum stopping targets forming muonic atoms. The stopped muons either decay into an electron and two neutrinos (Decay-In-Orbit, or DIO) or are captured by the nucleus. They are allowed in the Standard Model. If new physics beyond the Standard Model exists, the muon to electron conversion could occur. A signal electrons from the neutrinoless muon to electron conversion have a single value of energy (104.97 MeV), whereas electrons from DIO have a certain distribution whose endpoint energy is almost same with the signal energy [5]. Therefore, the main detector, CyDet is required to have a good energy resolution to separate the signal electrons from the DIO electrons.

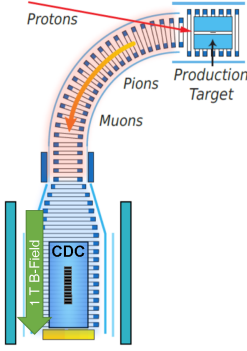


Figure 1: COMET Phase-I layout.

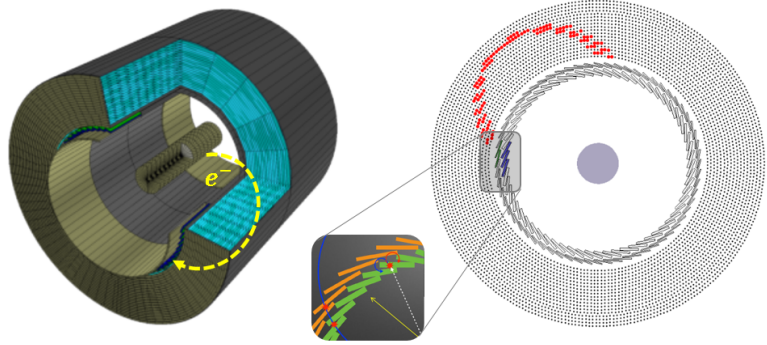


Figure 2: CyDet image (left) and the display of e^- event with the four-fold coincidence in a transverse cross section.

CyDet is composed of two detectors: the cylindrical drift chamber (CDC) and the CyDet trigger hodoscope (CTH). The electrons emitted from the stopping targets make a helix under the 1 T magnetic field and ionize the gas molecules while passing through the CDC filled with the gas mixture of He (90 %) and C_4H_{10} (10 %). The induced currents from ionized electrons and ions are recorded by the stereo sense wires arranged along the eighteen layers. The data is recorded only when the emitted electrons hit the CTH locating at both ends of the CDC, which provides a trigger. The CTH consists of the scintillators and Cherenkov detectors to discriminate the other types of particles, and it is triggered with four-fold coincidence where two of each detector are hit, as shown in Fig. 2.

1.2 Track finding challenge in COMET Phase-I experiment

There are two event types for the muon to electron conversion in CDC: a single turn and multiple turn event as displayed in Fig. 3. The purpose of particle tracking in the COMET experiment, which includes the process of track finding and track fitting, is finding the momentum of the first turn partition of the electron track, where the energy loss is minimal. Therefore, it is convenient to regard each turn partition as a different track during the particle tracking. Following this consideration, it is not difficult to pick up the hits belonging to the specific turn partition in the case of the single turn events because there exists only one turn partition in them*. Tracking seed information including the position and momentum can also be

*It is assumed that the hits from the beam backgrounds are almost negligible considering the efficiency of machine learning method developed for COMET [6].

obtained using the $z - \phi$ plot and stereo information, followed by the helix fitting.

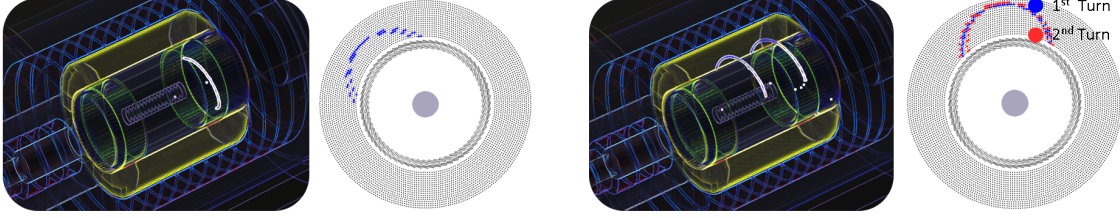


Figure 3: The event display of the single turn event (left) and Multiple, or double, turn event (right).

However, in the case of the multiple turn events, the track finding gets more complicated. The main problem is that there are too many combinations of hits which can be assigned for a specific turn partition. The implementation of the helix fitting to obtain the tracking seeds is also not proper because it does not account for the multiple scattering in the wires and inhomogeneous magnetic field.

In this paper, we introduce the track finding method which scans the set of the possible tracking seeds, rather than the set of hit combinations, and generates the Runge-Kutta fourth order tracks from the seeds to classify the hits nearby. Since the number of seeds to be scanned is still not small, GPGPU with CUDA [2] was utilized to achieve the reasonable computing speed. In Sec. 2, the scanning method will be explained both for the algorithm and GPGPU (CUDA) implementation. The results from the scanning method will be shown at Sec. 3, and Sec. 4 will introduce some technical aspects regarding on the CUDA implementation. Conclusions and outlooks will follow at Sec. 5.

2 GPGPU Scanning Method with Runge-Kutta Track

2.1 Preparing the set of the seeds

The seed of the track is supposed to have six track parameters: three for the position (\vec{x}_0) and three for the momentum (\vec{p}_0). If the cylindrical coordinate is used for the position, the radial component can be fixed to the radius (50 cm) of the inner wall of the CDC, therefore, the actual number of parameters to be scanned is five. The scanning range of the transverse scanning seeds (θ_0, p_{x0}, p_{y0}) is determined by the circle fitting method, namely the Hough transform. The resolution of the Hough transform was about 0.01 radian for θ_0 and 2.5 MeV for p_{x0} and p_{y0} , respectively. The determination of the scanning range of the longitudinal seeds (z_0, p_{z0}) utilizes the fixed location of the CTH as if it were a vertex detector. In other words, all electron signals recorded reach the CTH at the end of its track meaning that there is a certain pattern in (z_0, p_{z0}) for the last turn partition. Similar pattern also exists for the preceding turn partitions of the multiple turn events as shown in Fig. 5, however, they can not be used in the first place because the total turn number of an event is not known. Hence the track finding starts from the last turn partition. The total scanning range was set to cover at least 90% of the monte-carlo truth values of the CTH triggering event samples, and the granularity of the seeds was set not to exceed the GPU memory capacity. With these conditions, the number of seeds was about few tens of thousand.

2.2 The scanning method and its GPGPU implementation

The scanning method is basically a process iterating over the prepared seeds: For each iteration, the track with the corresponding seed propagates to find the DCA (distance of the closest approach) to the drift circles of all fired wires. The propagation of the track parameters is done with the STEP algorithm [7] based on the Runge-Kutta fourth order method. Then, we can evaluate the goodness of each seed by calculating the chi-square like value (E) defined by

$$E = \sum_{\text{wires}} \min(d_L^2, d_R^2, \lambda), \quad (1)$$

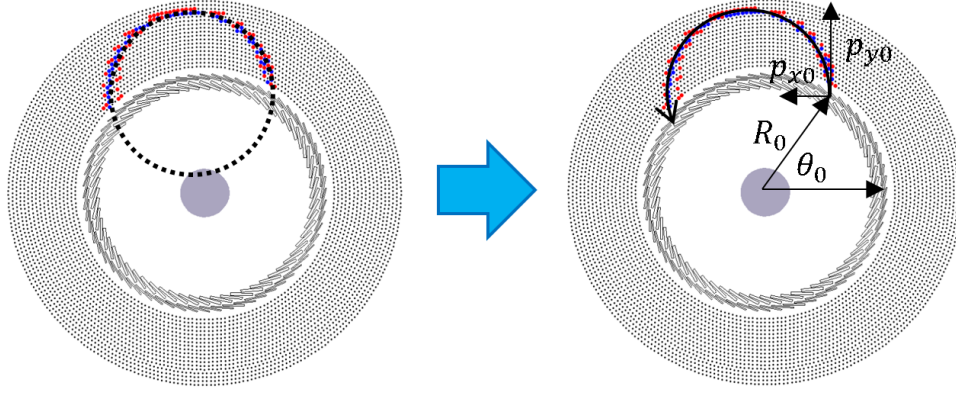
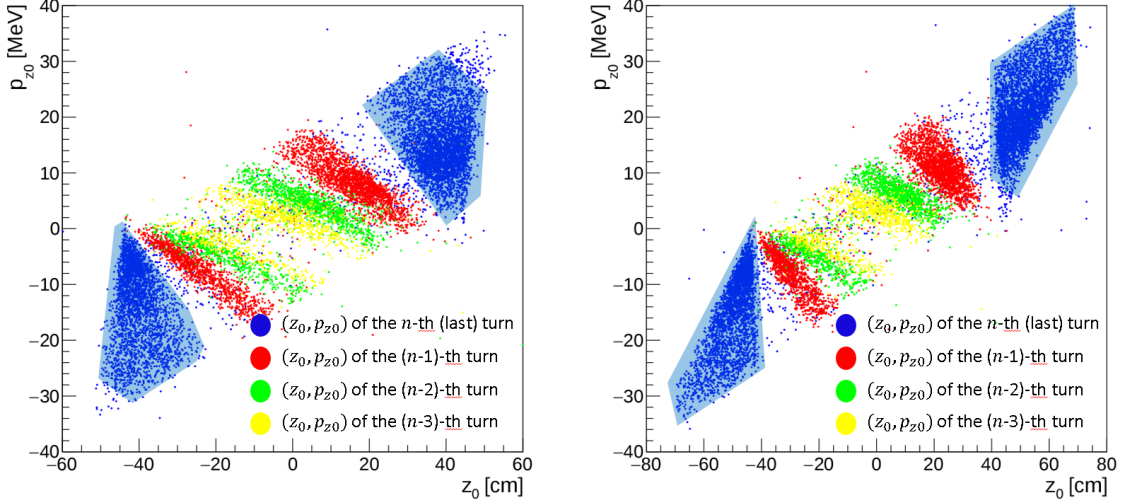


Figure 4: Extracting transverse seeds from the circle fitting.

Figure 5: The distribution of (z_0, p_{z0}) at the CDC entrance (left) and exit (right) of the multiple turn events

where d_L and d_R are DCA to the left and right side of the drift circle, respectively, which are from the left-right ambiguity. λ is the cutoff value ($O(10^{-3}) \text{ cm}^2$) to ignore the hits from the other turn partitions. After calculating E for all seeds, we took the several candidate seeds with the lowest E , and make other seed sets around them with finer granularity. Afterwards, the same scanning process was repeated ten times to get enough resolution for the seed selection. The hits whose square of DCA is less than the cutoff value ($d^2 < \lambda$) was classified as the hits of the turn partition being investigated.

Because the effect from the multiple scattering is less trivial when the extrapolation length gets longer, the track finding with the bidirectional extrapolation was adopted to mitigate these effects. It means that the scanning method was done for both seed sets of the CDC entrance and exit independently. The quality cut that the number of hits commonly found from the both direction (N_c) should be larger than or equal to 25 was applied to remove the misleading track finding results. The tracking finding results including the best seed and the hit classification were used for the track fitting with the Kalman filtering method [8].

Since a huge amount of the computation was required to process the scanning method with CPU, the CUDA was employed to parallelize the algorithm. The calculation of the GPU is performed by the threads, which is the smallest parallelizable unit, through the CUDA kernel function. The threads are grouped as a block, and the GPU can operate the multiple units of blocks concurrently. In the scanning method, each tracking seed is delivered to each block, and each thread in a block calculate the DCA for each wire (see

Fig. 6) Therefore, the number of blocks to be launched in the GPU is same with the number of scanning seeds, and the number of threads in a block with the number of the fired wires. The more detailed algorithm which was implemented to the GPU is described with more details in Sec. 4. Before launching the kernel function, the necessary information such as the magnetic field, the hit data, and the seeds is transferred to the global memory of the GPU, which has a few of GB capacity and can be accessed from any thread in any block. The track finding results are also stored at the global memory, and the GPU transfer them back to the CPU. A disadvantage of the global memory is that it has a small memory access speed compared to the CPU. The other variables generated during the STEP algorithm is stored at local memory whose access is confined to a certain thread but still as slow as global memory. Even though there is a shared memory residing on the GPU chip whose access speed is comparable to the CPU, it was not exploited as more shared memory allocation leads less number of blocks being launched simultaneously. The K40 and K80 model of the NVIDIA Tesla family [3] were tested to benchmark the algorithm performance.

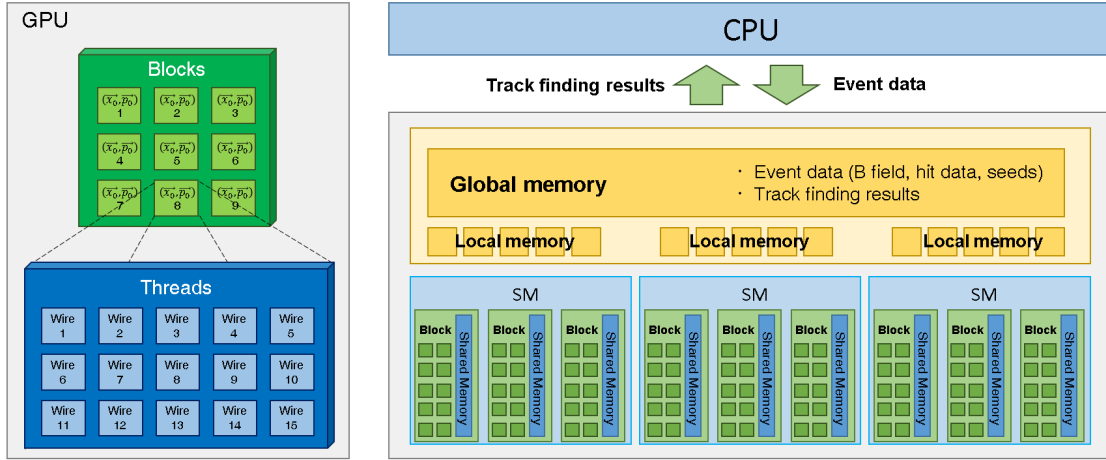


Figure 6: Schematic view of the GPGPU algorithm (left) and the memory hierarchy (right).

2.3 Full event reconstruction

Since the entrance momentum at the first turn partition is the closest to the vertex momentum with the minimal energy loss, each turn partition should be fitted from the last turn partition backwardly until we reconstruct the first turn partition. For the neighboring previous turn partition, most of track finding and fitting process is same with that of the last turn partition except the preparation of the longitudinal seed (z_0, p_{z0}) . The longitudinal seed at the entrance and the exit was predicted by backwardly-extrapolating the track of the next turn partition which was already fitted. The resolution of z_0 and p_{z0} , were 2.6 cm and 1.7 MeV, respectively, which are much better than the distribution shown in Fig. 5. The scanning method for the previous turn partition continued until the number of remaining unclassified hits becomes less than ten.

3 Results

3.1 Track finding results

The quality of the track finding with the scanning method can be quantified by the classification efficiency (ϵ) and purity (π) for the n' -th turn partition:

$$\epsilon_{n'} = \frac{C_{n' \rightarrow n'}}{C_{n'}}, \quad (2)$$

$$\pi_{n'} = \frac{C_{n' \rightarrow n'}}{\sum_{i=1}^n C_{i \rightarrow n'}}, \quad (3)$$

where n is the number of turns for an event, $C_{n'}$ is the total number of the hits from the n' -th turn partition, and $C_{i \rightarrow n'}$ is the number of the hits of the i -th turn partition classified as the hits of the n' -th turn partition. For example, the two dimensional histogram of Fig. 7 shows ϵ_n and π_n of the CTH triggering events after applying the quality cut of $N_c \geq 20$. The averages of ϵ_n and π_n were 76 % and 90 %, respectively.

The GPU scanning method was also compared with CPU-only scanning method by serializing all algorithms explained at Sec. 4. As shown in Fig. 8, it turned out that the speed of K40 and K80 was 33 and 26 times faster than the CPU (Intel E5-2620), respectively.

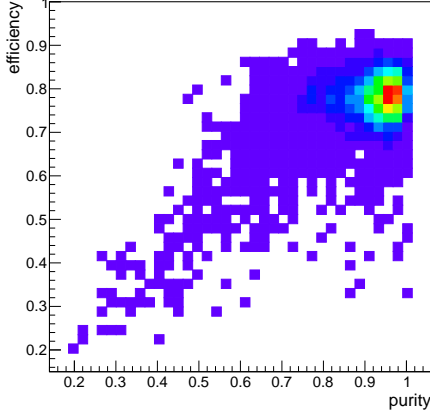


Figure 7: The two dimensional histogram of the efficiency and purity of the scanning method.

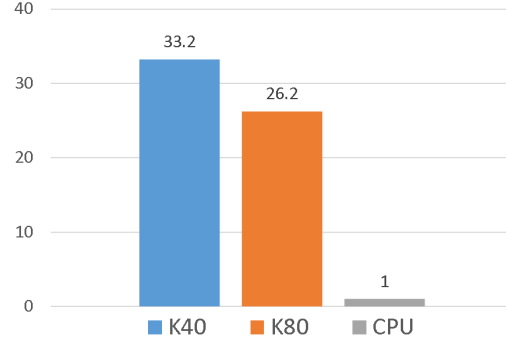


Figure 8: The speed of the GPU (K40 and K80) normalized to the speed of the CPU.

3.2 Track fitting results

The track fitting results shown at Fig. 9 represent the momentum distribution of the first turn partition, or the closest one to the first turn partition. Four of track quality cuts were given: 1) CTH triggering, 2) $N_c \geq 20$, 3) $NDF \geq 35$, and 4) $\chi^2/NDF \leq 2$. In the momentum residual histogram, the energy resolution for the core part was about 300 keV with the gaussian fitting. The tracking efficiency was defined as the number of events that pass the quality cuts divided by the number of CTH triggering events whose average number of hits per turn is larger or equal to 35, which is same with NDF cut. With the definition, the tracking efficiency for the single turn events and multiple turn events were 83% and 75%, respectively. Meanwhile, a broader low residual tail can be found in the histogram of the multiple turn events, compared with the single turn events. It is because few events were failed in reconstructing the first turn event ending up with more energy loss in the lastly fitted turn partition.

4 Technical Aspects

4.1 Limiting factors

The performance of the GPU usually gets better when more GPU resources are occupied, and the occupancy is proportional to the number of the fired wires of the events, corresponding to the number of threads. Therefore, the occupancy is low for the events with small number of the hits. Another issue is the branch divergence where some threads do not operate while the others do, which lowers the efficiency of the GPU utilization. The branch divergence occurs when threads do not have the same branching behavior, and it is inevitable due to the feature of the STEP algorithm where some threads can finish their jobs earlier, or later than others. The other issue, the main limiting factor, is the memory throttle occurred by the large memory

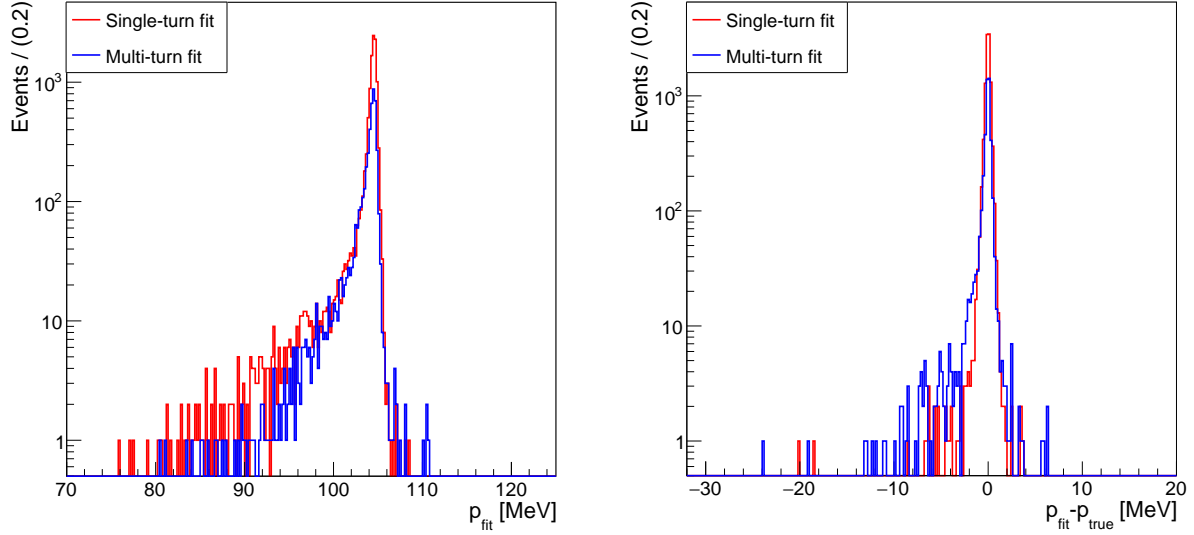


Figure 9: The histogram of the fitted momentum (left) and its residual (right) against the truth momentum at the first CDC entrance. The red and blue histogram represent the single turn events and multiple turn events, respectively.

bandwidth whose the biggest contribution is the magnetic field loading during the STEP algorithm. Figure 10 shows the GPU utilization status for each category and stall reasons, indicating that the large memory bandwidth and its comparatively low utilization is slowing the computation.

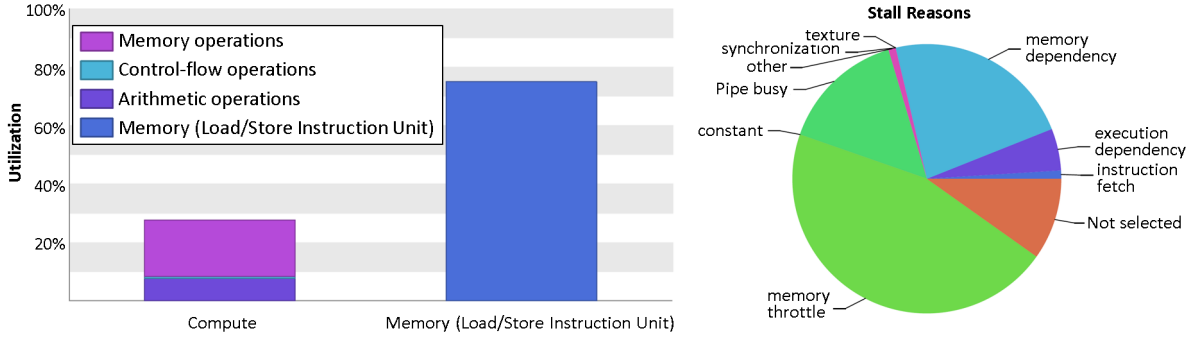


Figure 10: The GPU utilization status for each category (left) and the stall reasons in the GPU (right). These plots were generated by NVIDIA Visual Profiler [9].

4.2 Optimizing the GPU utilization

To minimize the effect from the branching divergence, the track finding algorithm to obtain the DCA wire was separated into two kernel functions. In the first kernel function, each seed was delivered to each thread, and recorded the track parameters of all steps during the Runge-Kutta extrapolation to the end of the turn partition. The algorithm of the second kernel function is same with what was described in Sec. 2.2, except that the track propagation of a thread starts from the recorded track parameter which is closest to the corresponding wire.

In terms of the memory management, the local memory allocation (e.g. the variable declaration in the

kernel function) was also reduced as much as possible to minimize the memory bandwidth. The optimization with more register memory (on-chip) that enhances the access speed to each thread was not employed as it reduces the number of blocks that can operate concurrently having the total efficiency drop. The shared memory was also not utilized for the same reason.

5 Conclusions and Outlooks

The track finding algorithm for the COMET Phase-I experiment using the modern GPU was introduced to achieve the good tracking resolution. The scanning method iterating over the set of possible tracking seeds showed the acceptable tracking resolution of 300 keV. However, the further optimization of many parameters such as the cut off value (λ) or the granularity of the seed sets over every iteration is required to increase tracking efficiency and resolution. The verification of the method should also be carried out by including the beam background hits which are not filtered by the pattern recognition, even though it would not effect much to the results. The background events of DIO, radiative muon capture and radiative pion capture as well as the other new physics processes such as $\mu^- \rightarrow e^+$ [10] will also be investigated.

ACKNOWLEDGEMENTS

This work was supported by IBS-R017-D1 of the Institute for Basic Science, the Republic of Korea.

References

- [1] W. H. Bertl *et al.* [SINDRUM II Collaboration], Eur. Phys. J. C **47**, 337 (2006).
- [2] J. Nickolls, I. Buck, M. Garland, and K. Skadron, ACM Queue **6**, 40–53 (2008).
- [3] E. Lindholm, J. Nickolls, S. Oberman, and J. Montrym, IEEE Micro **28**, 39–55 (2008).
- [4] G. Adamov *et al.* [COMET Collaboration], [arXiv:1812.09018 [physics.ins-det]].
- [5] A. Czarnecki, X. Garcia i Tormo, and W. J. Marciano, Phys. Rev. D **84**, 013006 (2011) [arXiv:1106.4756 [hep-ph]].
- [6] E. Gillies, A PhD thesis, Imperial College London, oct 2018.
- [7] E. Lund, L. Bugge, I. Gavrilenko and A. Strandli, JINST **4**, P04001–P04001 (2009).
- [8] T. Bilka *et al.*, [arXiv:1902.04405 [physics.data-an]].
- [9] NVIDIA Visual Profiler, <https://developer.nvidia.com/nvidia-visual-profiler>.
- [10] B. Yeo, Y. Kuno, M. Lee, K. Zuber, Phys. Rev. D **96**, 075027 (2017) [arXiv:1705.07464 [hep-ex]].